Rubidium Fluoride Post-Deposition Treatment: Impact on the Chemical Structure of the $Cu(In,Ga)Se_2$ Surface and $CdS/Cu(In,Ga)Se_2$ Interface in Thin-Film Solar Cells

Dagmar Kreikemeyer-Lorenzo[1], Dirk Hauschild[1,2,3,*], Philip Jackson[4], Theresa M. Friedlmeier[4], Dimitrios Hariskos[4], Monika Blum[5,6], Wanli Yang[5], Friedrich Reinert[3], Michael Powalla[4], Clemens Heske[1,2,6], and Lothar Weinhardt[1,2,6,*]

[1] Institute for Photon Science and Synchrotron Radiation (IPS), Karlsruhe Institute of Technology (KIT), Hermann-v.-Helmholtz-Platz 1, 76344 Eggenstein-Leopoldshafen, Germany

[2] Institute for Chemical Technology and Polymer Chemistry (ITCP), Karlsruhe Institute of Technology (KIT), Engesserstr. 18/20, 76128 Karlsruhe, Germany

[3] Experimental Physics VII, University of Würzburg, Am Hubland, 97074 Würzburg, Germany

[4] Zentrum für Sonnenenergie- und Wasserstoff-Forschung Baden-Württemberg (ZSW), Meitnerstrasse 1, 70563 Stuttgart, Germany

[5] Advanced Light Source (ALS), Lawrence Berkeley National Laboratory, One Cyclotron Road, Berkeley, CA 94720, USA

[6] Department of Chemistry and Biochemistry, University of Nevada, Las Vegas (UNLV), 4505 Maryland Parkway, Las Vegas, NV 89154-4003, USA

*Authors to whom correspondence should be addressed: dirk.hauschild@kit.edu, lothar.weinhardt@kit.edu

Keywords: $Cu(In,Ga)Se_2$, thin films, CIGSe solar cell, RbF post-deposition treatment, soft x-ray spectroscopy, photoelectron spectroscopy, high efficiency, chemical structure

Abstract

We present a detailed characterization of the chemical structure of the $Cu(In,Ga)Se_2$ thin-film surface and the $CdS/Cu(In,Ga)Se_2$ interface, both with and without a RbF post-deposition treatment (RbF-PDT). For this purpose, x-ray photoelectron and Auger electron spectroscopy, as well as synchrotron-based soft x-ray emission spectroscopy have been employed.

Although some similarities with the reported impacts of light-element alkali PDT (i.e., NaF- and KF-PDT) are found, we observe some distinct differences, which might be the reason for the further improved conversion efficiency with heavy-element alkali PDT. In particular, we find that the RbF-PDT reduces, but not fully removes, the copper content at the absorber surface, and does not induce a significant change in the Ga/(Ga + In) ratio. Additionally, we observe an increased amount of indium and gallium oxides at the surface of the treated absorber. These oxides are partly (in the case of indium) and completely (in the case of gallium) removed from the CdS/Cu(In,Ga)Se_2 interface by the chemical bath deposition of the CdS buffer.

I. INTRODUCTION

The presence of alkali elements, such as sodium and potassium, has proven crucial for the development of Cu(In,Ga)Se_2 (CIGSe) solar cells with high conversion efficiencies [1–19]. In fact, sodium is present in the production of every high-efficiency CIGSe solar cell [1–8], either by diffusion from the soda-lime glass or by deliberate introduction during the absorber production process. The efficiency of CIGSe-based solar cells has experienced a further boost by the introduction of a potassium fluoride (KF) post-deposition treatment (KF-PDT) [9]. Since then, many efforts have been made to understand the mechanism(s) of this treatment, and to control and optimize its effect on the buffer layer/absorber interface [10–18]. With a KF-PDT process step, CIGSe-based solar cells achieved efficiencies close to 22%, overtaking the long-standing efficiency record held by polycrystalline silicon lab-scale solar cells [20,21]. Probably one of the most important findings of this breakthrough is that KF-PDT often leads to a depletion or complete removal of copper at the surface of the CIGSe absorber [9,11–14,17]. While a similar gallium depletion has been reported [9,17], an increase of the gallium content has also been observed [11]. In addition, KF-PDT allows for using thinner CdS layers [9,10,16,22]. More recently, another increase of solar cell efficiency (significantly above 22%) has been reached

by employing post-deposition treatments with heavier alkali elements, namely rubidium fluoride (RbF-PDT) and cesium fluoride (CsF-PDT) [19,23–25].

Here, we report on the impact of the RbF-PDT on the chemical structure of the CIGSe absorber surface, the CdS buffer layer, as well as the CdS/CIGSe interface (a corresponding study of its impact on the electronic structure, including the band alignment, can be found in Ref [19]). Using a combination of x-ray photoelectron spectroscopy (XPS), x-ray-excited Auger electron spectroscopy (XAES), and synchrotron-based soft x-ray emission spectroscopy (XES), we can paint a detailed picture of the influence of the RbF-PDT on the absorber surface and the buffer/absorber interface.

II. EXPERIMENTAL DETAILS

Two different sets of samples were prepared by the Zentrum für Sonnenenergie- und Wasserstoff-Forschung Baden-Württemberg (ZSW). The absorbers were prepared by co-evaporation of Cu, Ga, In, and Se in a multistage process on a thin film of sputtered molybdenum on a soda-lime glass substrate [21]. Subsequently, one of the two sample sets underwent a RbF-PDT (as described in [20,21]). Both sets of samples consist of a bare CIGSe absorber and three CdS/CIGSe samples with different chemical bath deposition (CBD) times (2, 90, and 180 s). Samples processed in a similar way as the PDT samples achieve a conversion efficiency of 22.6 % .

All CIGSe samples were taken out of the high-vacuum growth chamber and exposed to air for less than 5 minutes. The “bare CIGSe” absorbers were then sealed under inert atmosphere and the rest of the samples were further processed. The samples with thin CdS were dried with pressurized nitrogen directly after the chemical bath and sealed under inert atmosphere immediately afterwards. All samples were transported to the University of Würzburg for XPS and XAES measurements, where they were transferred to the ultra-high-vacuum chamber without further exposure to ambient air. The measurements were carried out with a VG CLAM 4 electron analyzer and a Mg K_α x-ray source. After the XPS measurements, the samples were sealed again under inert atmosphere and shipped for

XES measurements to the Advanced Light Source (ALS) at the Lawrence Berkeley National Laboratory, where they were briefly exposed to air (less than one minute). The samples were measured at the SXF endstation at beamline 8.0.1 [26]. The base pressure in the XPS and XES chambers was less than $5x10^{-10}$ and $2x10^{-9}$ mbar, respectively.

III. RESULTS

To study the native oxides and adsorbates of the surfaces with and without PDT, we have investigated samples *without* any additional surface cleaning steps (such as our customary low-energy ion treatment). This is in contrast to our work in Ref. [19], where the *electronic structure* was investigated, for which a low-energy ion-treatment was necessary to correctly determine the band alignment at the interface.

Figure 1 shows the Mg K_α XPS survey spectra for the CIGSe absorbers ("0 s") and the CdS buffer layers after different CBD times (2, 90, and 180 s), corresponding to increasing CdS thickness. The spectra of the untreated and treated samples are presented in black and red, respectively. With increasing CdS deposition time, the characteristic lines for CIGSe (e.g., Cu 2p, In 3d, Ga 2p, and Se 3d) are attenuated, and the CdS-related lines (e.g., Cd 3d and S 2p) increase gradually, as expected. Moreover, sodium-related features are visible for all samples, which can be related to diffusion from the soda-lime glass substrate [27]. This sodium signal decreases with increasing buffer layer thickness. A rubidium-related signal (Rb 3d) is also observed for the treated samples and will be shown and discussed in conjunction with Fig. 2, while no residual fluorine signal could be detected. For the bare absorber (bottom spectra), we observe a difference in the shape of the O 1s peak (Figure S.I.1), suggesting the presence of (at least) a second oxygen species. After 2 s of CdS CBD, this/these additional species is/are almost completely removed.

In the following, the impact of the RbF-PDT treatment on the CIGSe surface is discussed. First, we find that the majority of the prominent peak intensities (e.g., of Ga 2p, In 3d, and Se 3d) remain constant after PDT.

To quantify the surface composition independently of changes in the surface adsorbate layer, we compute the Ga/(Ga+In) (GGI) ratio using the In 4d and Ga 3d signal intensities and calculated photoionization cross sections[28]. For these lines, the inelastic mean free paths and analyzer transmission are nearly identical, due to their very similar kinetic energies. We find no change of the surface GGI ratio (0.35 ± 0.05) with and without the PDT. This is in contrast to some of the previous KF studies[9,17] that suggest an almost complete removal of gallium from the surface. In a similar fashion, we calculated the Se/(Se+In+Ga) (SSIG) surface ratio (using the Se 3d, In 4d, and Ga 3d lines). Here, we find an SSIG of 0.52 ± 0.07 for both samples, i.e., also independent of the PDT.

Different from the Ga, In, and Se signals, we find a significant *decrease* of the Na 1s and Cu 2p intensities after RbF-PDT. Using the Cu 3p, In 4d, and Ga 3d lines, we determine a reduced Cu/(In+Ga) (CIG) ratio of 0.34 (± 0.09) at the surface [from 0.44 (± 0.09) before RbF-PDT]. Nevertheless, in contrast to studies suggesting a *complete* removal of Cu from the surface by alkali fluoride treatments [9,11,13,14,17], the Cu 2p signal is still well visible (as was found for KF-PDT on industrial CIGSSe absorbers [18]). Finally, we note a significant increase of the C 1s intensity, indicating additional carbon-containing adsorbates after PDT.

With increasing CdS chemical bath deposition time, the absorber-related XPS features are attenuated. After 180 s of CBD on the RbF-PDT absorber, no absorber-related lines are visible, while most of them can still be observed for the same CBD deposition time on the untreated absorber (except for the Ga 2p electrons, which have the lowest kinetic energy and thus shortest attenuation length). The fact that no absorber lines are seen for the PDT sample after 180 s of CBD suggests the formation of a closed CdS layer, while the layer is likely not fully closed (or in places very thin) after the identical deposition time without prior RbF-PDT (for further details, including SEM pictures, see Ref. [22]).

Although the Na 1s electrons have a very short inelastic mean free path of $\lambda \sim 0.7$ nm [29], the corresponding peak is observable for all CdS thicknesses with and without RbF-PDT, indicating either a diffusion of the (highly mobile) sodium[30] through the CdS buffer layer towards the oxygen-

containing surface (see below), and/or a re-adsorption from the CdS bath (e.g., during removal of the sample). Furthermore, we observe a slightly larger sodium signal for all untreated samples; this could be due to a multitude of reasons, including the hypothesis that heavy alkali elements can replace lighter alkali elements at the surface during RbF-PDT [21]. The modified Auger parameter (α') for sodium is similar for all samples (α'~ 2061.6 eV), which is in the range often found for sodium on CIGSe surfaces [31–35]. For the treated and untreated absorber surfaces, which also exhibit a carbonate-related feature in the C 1s peak (Figure S.I.1.), we ascribe this sodium species to Na_2CO_3 [α'(Na_2CO_3) = 2061.2 – 2061.7 eV] [32,33,35]. For the samples with CdS layer, a carbonate signal is also found (Figure S.I.1.). Additionally, sodium sulfite or sulfate[36] [α'(Na_2SO_3) = 2061.6 – 2061.7 eV, or α'(Na_2SO_4) = 2061.0 – 2061.9 eV)] [37–39] could be present as well.

To further investigate the impact of the RbF-PDT on the formation of the CdS/CIGSe interface, we have studied the Ga 3p/Rb 3d/Cd 4s spectral region. Figure 2 shows data and fits of this region for the full PDT sample set and two of the untreated samples (0 and 180 s CdS). The Fityk peak fitting software [40] was used to perform the fit simultaneously for the entire data set using linear backgrounds and Voigt profiles, where the Lorentzian and Gaussian widths were kept fixed for the same element. The ratio between spin-orbit split lines was fixed according to their multiplicity (2j+1), and the same peak separation was used throughout the entire data set. As expected, no rubidium signal can be found on the untreated samples. The treated bare absorber shows a significant Rb 3d intensity (approx. 1% elemental ratio at the surface), which decreases with CdS deposition time, while the Cd 4s line increases in intensity. The rubidium signal is still relatively large for the 90 s sample, and, although very small, still present for the 180 s sample. To display this, we have generated a weighted difference between the spectra of the 180 s CdS samples with and without treatment (Figure 2, blue spectrum). The difference spectrum clearly shows spectral intensity at ca. 111 eV, indicating the presence of (small amounts of) Rb. In contrast, there is no evidence for a residual Ga 3p signal (at ca. 105.5 eV), despite the very similar inelastic mean free

path. The finding of a Rb 3d signal even for the thickest CdS layer thus suggests a (weak) diffusion of rubidium into the CdS layer. In a previous study of Na in In_xS_y buffer layers, an increase in solar-cell efficiency due to an alkali-induced increase in the buffer-layer band gap was found.[41] Similarly, in our current case, Rb atoms in the buffer layer may contribute to the observed increased band gap of the CdS buffer layer. [19]

In the two upper spectra (180 s CdS with and without PDT), we observe a second Cd 4s component at ~114.2 eV (purple curve in Figure 2, labeled "Cd 4s'"). We assign this feature to a cadmium species in an oxidic environment, which is supported by a second component in the Cd MNN Auger spectra (see text below) and the finding of O signals at the buffer-layer surfaces.

To determine the local chemical environment of the indium and gallium atoms, Figure 3 shows XAES spectra of indium ($M_{4,5}N_{4,5}N_{4,5}$) and gallium ($L_3M_{4,5}M_{4,5}$) for the absorber and the thinnest CdS layer with and without PDT. All four In MNN spectra can be well described with two spectral components, as shown in Fig. 3 (left). Using a single-species In MNN spectrum (derived from a sputter-cleaned In foil) as a reference, a two component analysis was performed to fit the In MNN spectra. Comparing with literature [42] and our own prior work, the prominent In component ($M_4N_{45}N_{45}$ at ~407.4 eV) is in accordance with a CIGSe environment. The second component is found at 405.0 eV for the untreated bare absorber and at 405.5 eV for the other samples, in accordance with an oxidic environment (e.g., $In(OH)_3$ or In_2O_3 [39,43]). The ratios between the oxidized and CIGSe components are (0.23 ± 0.05) for the untreated absorber and (0.30 ± 0.05) for the PDT absorber. The relative intensity of the oxidic component is reduced by a factor of 3 after 2 s CBD for the treated sample, whereas it only slightly decreases for the untreated one.

In the case of gallium (Fig. 3, right), the spectrum after 2 s CdS CBD shows a predominantly single-species line shape, as derived from a comparison to reference Ga LMM spectra [39]. In contrast, the spectra of the treated and untreated absorbers clearly show a second component at ca. 1062 eV. To visualize the second component, the results of two-component fits are shown in Figure 3. For these fits, the 2 s CdS untreated sample was taken

as the single-species reference spectrum. The observed second component is in accordance with the presence of Ga_2O_3, and is considerably larger for the PDT sample. Furthermore, we note that it is entirely removed after 2 s of CdS CBD (for both absorbers). While the PDT increases the amount of oxides at the surface, they are easily removed during the CdS-CBD. We surmise that this could be beneficial for the CdS growth.

Figure 4 shows the Cd $M_{4,5}N_{4,5}N_{4,5}$ XAES spectrum for the RbF-PDT 180 s CdS sample, together with a two-component fit. The Cd MNN spectrum of the untreated 180 s CdS sample looks identical to the RbF-PDT spectrum, except for a small shift in energy (0.05 eV), which is not shown here. Two fit components (gray color) were needed to reproduce the cadmium spectrum: the Cd MNN spectrum of a cleaned CdS reference sample and the same spectrum scaled and shifted to lower kinetic energy. The sum of these two components is represented by the red curve. Literature values for the prominent $M_4N_5N_5$ peak of cadmium-containing compounds are shown above the spectra. The first component at ~380.9 eV corresponds to CdS, whereas the second component, shifted ~0.8 eV towards lower kinetic energy, indicates the presence of an O-containing species, either $CdSO_4$ or $Cd(OH)_2$ [38,39]. In conjunction with this, the S 2p core level shows an oxidized sulfur species with the corresponding chemical shifts (to 167.1 or 168.7 eV, resp.) for the treated and untreated samples (Figure 5), which is in accordance with the formation of $CdSO_4$. We hence identify an oxygen-containing component in the CdS CBD layer (and not just an adsorbate layer *on* the CdS surface), which is likely the reason for the large electronic CdS surface band gap (2.60 ± 0.14 eV) observed for these samples [19].

For further analysis of the chemical structure of the sample series, XES spectra of the S $L_{2,3}$ emission of the two 180 s samples (spectral region of the upper valence band magnified by a factor of 10) were taken. Different from the surface-sensitive XPS and XAES data discussed above, the here presented XES data are governed by the 1/e attenuation length of the

incoming (approx. 100 nm) and emitted (approx. 380 nm) x-rays at the S $L_{2,3}$ edge[44], and thus probes the entire CdS film. The spectra of the two samples are compared with the spectra of CdS, Rb_2SO_4, Na_2SO_4, and $CdSO_4$ reference samples in Figure 6 (note the magnification factors for the upper valence band region). The characteristic features of CdS are observed (for both 180 s CBD samples) at ~147.5 eV (S 3s → S 2p), at 150.7 eV and 151.9 eV (Cd 4d-derived bands → S 2p), and around 156.5 eV (upper valence band → S 2p) [45]. All features appear more pronounced for the CdS reference spectrum, which we attribute to a higher degree of order for this single crystal sample (as compared to the CBD CdS thin films). Moreover, the CdS/CIGSe samples exhibit a feature at ~162.5 eV that is not present in the CdS reference spectrum. At or near this energy, S 3d → S 2p transitions are typically found for sulfate or sulfite compounds [36,46]. The sulfate reference spectra show two sharp lines at lower emission energy, attributed to S 3s → S 2p transitions. These transitions overlap with the upper valence band of the two CBD CdS samples, and hence they are difficult to be discerned. To do so, Fig. 6 also shows a magnified (x50) difference spectrum (PDT – no PDT); while the signal-to-noise level is low, characteristic spectral features of S-O bonds are nevertheless visible. We thus argue that the two CBD CdS samples presented here contain S in a higher oxidation state, as also inferred from the XPS results. Note that sulfate and sulfite species have been shown to be instable in the x-ray beam: they can either form (if sufficient amounts of water or hydroxides are present in the film [47,48]) or be disintegrated [36].

IV. SUMMARY

Using XPS, XAES, and XES, we have studied the chemical structure of the CdS/CIGSe interface as present in high-efficiency thin film solar cells with and without post-deposition treatment (PDT). We find a significant amount of rubidium at the absorber surface after the PDT. Furthermore, we find a reduction of the copper content, but no difference in the GGI (“gallium to (gallium plus indium)”) ratio at the surface after the RbF-PDT treatment. After the chemical bath deposition, we find evidence for a diffusion of

rubidium and sodium towards the surface of the buffer layer. All samples with PDT show lower sodium signals, suggesting that heavy alkali elements can replace lighter ones. In addition, larger amounts of indium and gallium oxides are present for the PDT absorbers. An oxidic cadmium species is observed for the RbF-PDT and the thickest untreated CdS/CIGSe interface samples. Finally, we find indications for sulfates and/or sulfites in the CBD-CdS buffer layer.

Although there are some similarities between the reported effects of a rubidium fluoride and a potassium fluoride treatment (e.g., “earlier” formation of a closed CdS layer) on CIGSe, RbF post-deposition treatment modifies the CIGSe surface in a different way than previously reported for KF treatments. In particular, we find a much weaker copper depletion at the surface, no changes in the GGI ratio, and an interplay between heavy and light alkali elements. These differences paint a complex picture of the particular nature of the RbF-PDT, and might give insights into potential optimization pathways to further optimize alkali PDTs.

Acknowledgments

This research used resources of the Advanced Light Source, which is a DOE Office of Science User Facility under contract no. DE-AC02-05CH11231. D.H., C.H., and L.W. acknowledge funding by the BMWi project “EFFCIS” (No. 0324076E). The ZSW acknowledges the CIS-ProTec project (FKZ 0325715A) and CISHiTec project (FKZ 0324179) for funding.

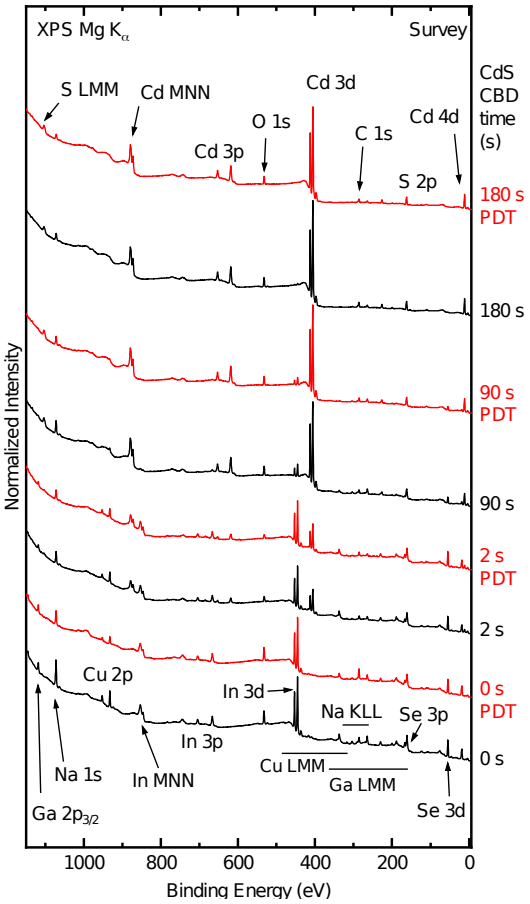

Figure 1: Mg K_α x-ray photoelectron survey spectra for CIGSe (labeled “0 s”) and CdS/CIGSe layers with varying CdS chemical bath deposition times (given on the right). Red curves denote samples after RbF-PDT, black curves denote samples without PDT of the absorber surface.

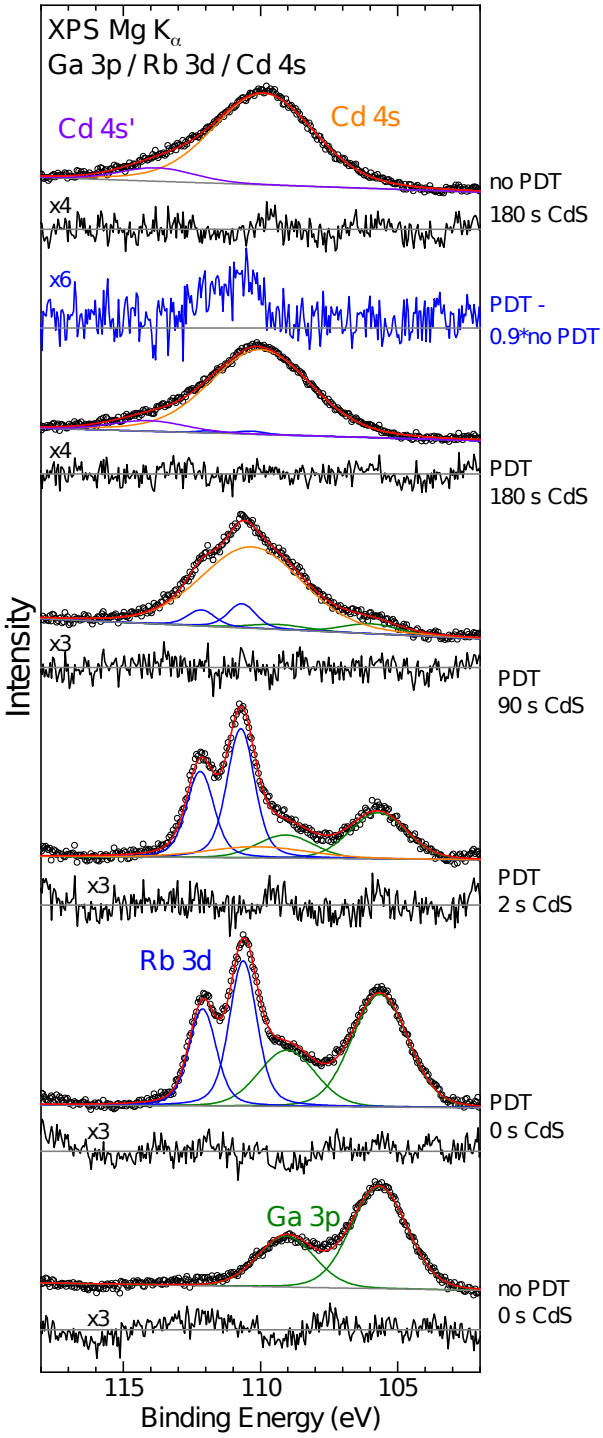

Figure 2: Mg K_α XPS detail spectra of the Ga 3p/Rb 3d/Cd 4s region of six selected samples. Colored curves show fit results, with individual components depicted in green (Ga 3p), blue (Rb 3d), orange (Cd 4s), and purple (Cd 4s'). Residuals are displayed in black below each spectrum, and are multiplied by a factor of 4 for the 180 s samples, and a factor of 3 for

all other samples. Between the two “180 s CdS” sample spectra, the difference between the CdS/PDT-CIGSe and 90% of the CdS/no PDT-CIGSe spectrum is shown in blue (multiplied by a factor of 6) to show the presence of a weak Rb 3d signal.

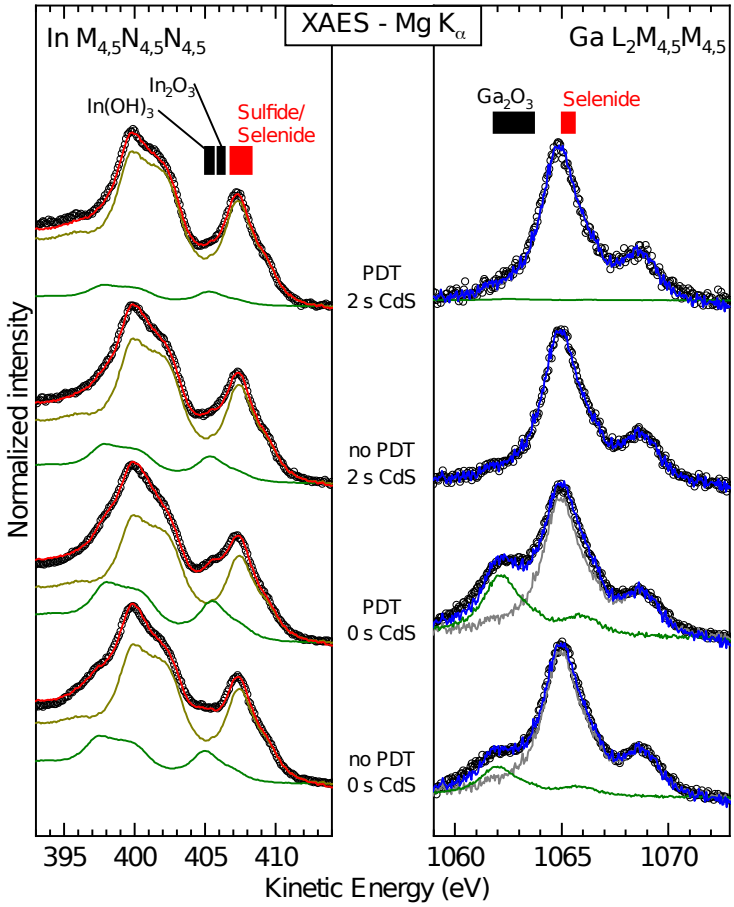

Figure 3: Mg K_α-excited XAES spectra of indium (left) and gallium (right) for the two bare absorbers (two bottom spectra) and the samples with 2 s CdS chemical bath deposition (two uppermost spectra). Raw data is represented as open black circles, individual species (fit components) are represented in green and gray colors, and the sum is displayed in red and blue for the indium and gallium spectra, respectively. Literature values for different compounds are depicted as boxes [38,39].

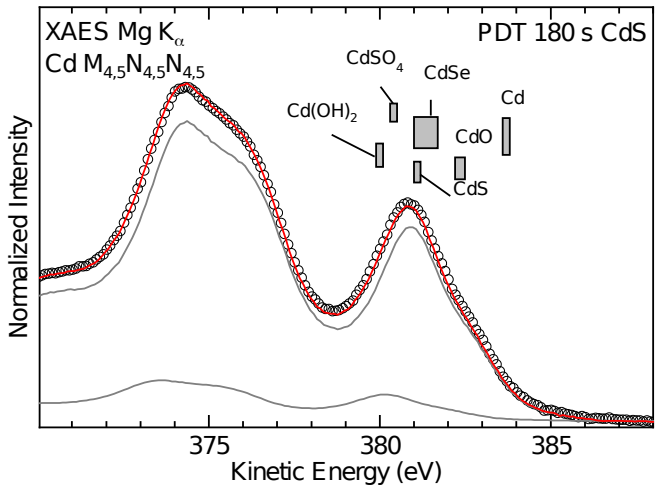

Figure 4: Mg K_α-excited Cd $M_{4,5}N_{4,5}N_{4,5}$ XAES spectra for the RbF-PDT 180 s CdS sample. Black circles denote the raw data, gray curves represent two fit components, and the sum is displayed in red. Literature values for different compounds are depicted as boxes [38,39].

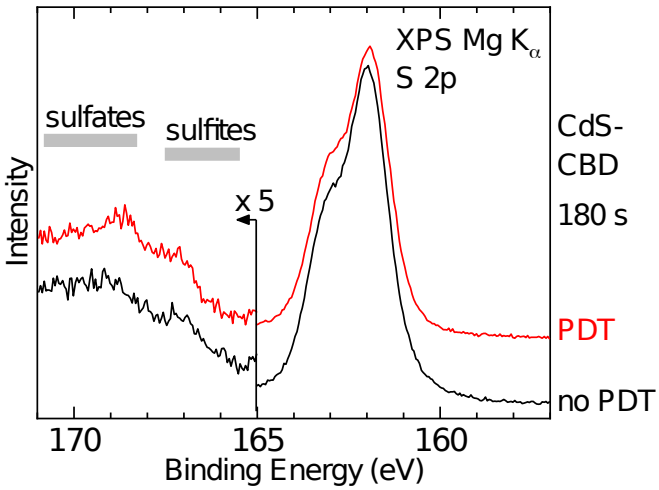

Figure 5: Mg K_α XPS spectra of the S 2p region for the treated (red) and untreated (black) CdS/CIGSe samples. The oxide region (binding energies above 165 eV) is magnified by a factor of 5. Literature values for sulfates and sulfites are depicted as boxes [38,39].

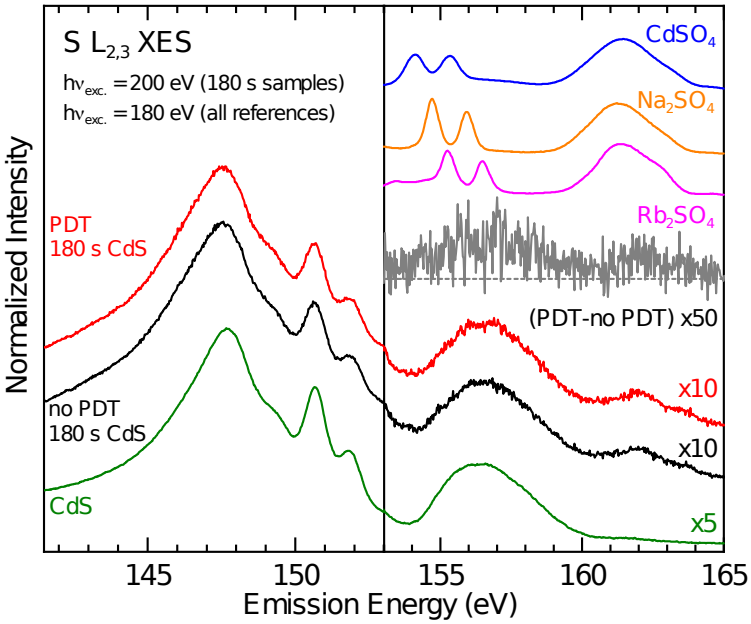

Figure 6: S $L_{2,3}$ XES spectra of the 180 s CdS/CIGSe samples ($h\nu_{exc.}$ = 200 eV) with and without PDT, as well as CdS, Rb_2SO_4, Na_2SO_4, and $CdSO_4$ references ($h\nu_{exc.}$ = 180 eV). The valence regions of the 180 s CdS/CIGSe samples and the CdS reference are magnified by a factor of 10 and 5, respectively. The difference spectrum of the 180s PDT – no PDT is also shown, magnified by a factor of 50 (right panel). The sulfate references are shown on an arbitrary intensity scale.

REFERENCES

(1) Heske, C.; Eich, D.; Fink, R.; Umbach, E.; van Buuren, T.; Bostedt, C.; Kakar, S.; Terminello, L. J.; Grush, M. M.; Callcott, T. A.; Himpsel, F. J.; Ederer, D. L.; Perera, R. C. C.; Riedl, W.; Karg, F. Semi-Quantitative and Non-Destructive Analysis of Impurities at a Buried Interface: Na and the CdS/Cu(In,Ga)Se_2 Heterojunction. *Surf. Interface Anal.* **2000**, *30*, 459–463

(2) Rudmann, D.; Brémaud, D.; da Cunha, A. F.; Bilger, G.; Strohm, A.; Kaelin, M.; Zogg, H.; Tiwari, A. N. Sodium Incorporation Strategies for CIGS Growth at Different Temperatures. *Thin Solid Films* **2005**, *480–481*, 55–60.

(3) Erslev, P. T.; Lee, J. W.; Shafarman, W. N.; Cohen, J. D. The Influence of Na on Metastable Defect Kinetics in CIGS Materials. *Thin Solid Films* **2009**, *517*, 2277–2281.

(4) Caballero, R.; Kaufmann, C. A.; Eisenbarth, T.; Cancela, M.; Hesse, R.; Unold, T.; Eicke, A.; Klenk, R.; Schock, H. W. The Influence of Na on Low Temperature Growth of CIGS Thin Film Solar Cells on Polyimide Substrates. *Thin Solid Films* **2009**, *517*, 2187–2190.

(5) R. Caballero; C. A. Kaufmann; T. Eisenbarth; A. Grimm; I. Lauermann; T. Unold; R. Klenk; H. W. Schock. Influence of Na on Cu(In,Ga)Se_2 Solar Cells Grown on Polyimide Substrates at Low Temperature: Impact on the Cu(In,Ga)Se_2/Mo Interface. *Appl. Phys. Lett.* **2010**, *96*, 092104.

(6) Wuerz, R.; Eicke, A.; Kessler, F.; Rogin, P.; Yazdani-Assl, O. Alternative Sodium Sources for Cu(In,Ga)Se_2 Thin-Film Solar Cells on Flexible Substrates. *Thin Solid Films* **2011**, *519*, 7268–7271.

(7) L. E. Oikkonen; M. G. Ganchenkova; A. P. Seitsonen; R. M. Nieminen. Effect of Sodium Incorporation into $CuInSe_2$ from First Principles. *J. Appl. Phys.* **2013**, *114*, 083503.

(8) Puttnins, S.; Levcenco, S.; Schwarzburg, K.; Benndorf, G.; Daume, F.; Rahm, A.; Braun, A.; Grundmann, M.; Unold, T. Effect of Sodium on Material and Device Quality in Low Temperature Deposited Cu(In,Ga)Se_2. *Sol. Energy Mater. Sol. Cells* **2013**, *119*, 281–286.

(9) Chirilă, A.; Reinhard, P.; Pianezzi, F.; Bloesch, P.; Uhl, A. R.; Fella, C.; Kranz, L.; Keller, D.; Gretener, C.; Hagendorfer, H.; Jaeger, D.; Erni, R.; Nishiwaki, S.; Buecheler, S.; Tiwari, A. N. Potassium-Induced Surface Modification of Cu(In,Ga)Se_2 Thin Films for High-Efficiency Solar Cells. *Nat. Mater.* **2013**, *12*, 1107–1111.

(10) Pianezzi, F.; Reinhard, P.; Chirilă, A.; Bissig, B.; Nishiwaki, S.; Buecheler, S.; Tiwari, A. N. Unveiling the Effects of Post-Deposition Treatment with Different Alkaline Elements on the Electronic Properties of CIGS Thin Film Solar Cells. *Phys. Chem. Chem. Phys.* **2014**, *16*, 8843–8851.

(11) P. Pistor; D. Greiner; C. A. Kaufmann; S. Brunken; M. Gorgoi; A. Steigert; W. Calvet; I. Lauermann; R. Klenk; T. Unold. Experimental Indication for Band Gap Widening of Chalcopyrite Solar Cell Absorbers after Potassium Fluoride Treatment. *Appl. Phys. Lett.* **2014**, *105*, 063901.

(12) Laemmle, A.; Wuerz, R.; Powalla, M. Investigation of the Effect of Potassium on Cu(In,Ga)Se_2 Layers and Solar Cells. *Thin Solid Films* **2015**, *582*, 27–30.

(13) Ümsür, B.; Calvet, W.; Steigert, A.; Lauermann, I.; Gorgoi, M.; Prietzel, K.; Greiner, D.; Kaufmann, C. A.; Unold, T.; Lux-Steiner, M. C. Investigation of the Potassium Fluoride Post Deposition Treatment on the CIGSe/CdS Interface Using Hard X-Ray Photoemission Spectroscopy – a Comparative Study. *Phys. Chem. Chem. Phys.* **2016**, *18*, 14129–14138.

(14) Aguiar, J. A.; Stokes, A.; Jiang, C.-S.; Aoki, T.; Kotula, P. G.; Patel, M. K.; Gorman, B.; Al-Jassim, M. Revealing Surface Modifications of Potassium-Fluoride-Treated Cu(In,Ga)Se_2: A Study of Material Structure, Chemistry, and Photovoltaic Performance. *Adv. Mater. Interfaces* **2016**, *3*, 1600013.

(15) S. A. Jensen; S. Glynn; A. Kanevce; P. Dippo; J. V. Li; D. H. Levi; D. Kuciauskas. Beneficial Effect of Post-Deposition Treatment in High-Efficiency Cu(In,Ga)Se_2 Solar Cells through Reduced Potential Fluctuations. *J. Appl. Phys.* **2016**, *120*, 063106.
(16) Lepetit, T.; Harel, S.; Arzel, L.; Ouvrard, G.; Barreau, N. Coevaporated KInSe2: A Fast Alternative to KF Postdeposition Treatment in High-Efficiency Cu(In,Ga)Se_2 Thin Film Solar Cells. *IEEE J. Photovolt.* **2016**, *6*, 1316–1320.
(17) Handick, E.; Reinhard, P.; Wilks, R. G.; Pianezzi, F.; Kunze, T.; Kreikemeyer-Lorenzo, D.; Weinhardt, L.; Blum, M.; Yang, W.; Gorgoi, M.; Ikenaga, E.; Gerlach, D.; Ueda, S.; Yamashita, Y.; Chikyow, T.; Heske, C.; Buecheler, S.; Tiwari, A. N.; Bär, M. Formation of a K—In—Se Surface Species by NaF/KF Postdeposition Treatment of Cu(In,Ga)Se_2 Thin-Film Solar Cell Absorbers. *ACS Appl. Mater. Interfaces* **2017**, *9*, 3581–3589.
(18) Mezher, M.; Mansfield, L. M.; Horsley, K.; Blum, M.; Wieting, R.; Weinhardt, L.; Ramanathan, K.; Heske, C. KF Post-Deposition Treatment of Industrial Cu(In, Ga)(S, $Se)_2$ Thin-Film Surfaces: Modifying the Chemical and Electronic Structure. *Appl. Phys. Lett.* **2017**, *111*, 071601.
(19) Hauschild, D.; Kreikemeyer-Lorenzo, D.; Jackson, P.; Friedlmeier, T. M.; Hariskos, D.; Reinert, F.; Powalla, M.; Heske, C.; Weinhardt, L. Impact of a RbF Postdeposition Treatment on the Electronic Structure of the CdS/Cu(In,Ga)Se_2 Heterojunction in High-Efficiency Thin-Film Solar Cells. *ACS Energy Lett.* **2017**, 2383–2387.
(20) Jackson, P.; Hariskos, D.; Wuerz, R.; Wischmann, W.; Powalla, M. Compositional Investigation of Potassium Doped Cu(In,Ga)Se_2 Solar Cells with Efficiencies up to 20.8%. *Phys. Status Solidi RRL.* **2014**, *8*, 219–222.
(21) Jackson, P.; Hariskos, D.; Wuerz, R.; Kiowski, O.; Bauer, A.; Friedlmeier, T. M.; Powalla, M. Properties of Cu(In,Ga)Se_2 Solar Cells with New Record Efficiencies up to 21.7%. *Phys. Status Solidi RRL.* **2015**, *9*, 28–31.
(22) T. M. Friedlmeier; P. Jackson; D. Kreikemeyer-Lorenzo; D. Hauschild; O. Kiowski; D. Hariskos; L. Weinhardt; C. Heske; M. Powalla. A Closer Look at Initial CdS Growth on High-Efficiency Cu(In,Ga)Se_2 Absorbers Using Surface-Sensitive Methods. *Proc 2016 IEEE 43rd Photovolt. Spec. Conf. PVSC* **2016**, 0457–0461.
(23) Jackson, P.; Wuerz, R.; Hariskos, D.; Lotter, E.; Witte, W.; Powalla, M. Effects of Heavy Alkali Elements in Cu(In,Ga)Se_2 Solar Cells with Efficiencies up to 22.6%. *Phys. Status Solidi RRL.* **2016**, *10*, 583–586.
(24) Nicoara, N.; Kunze, T.; Jackson, P.; Hariskos, D.; Félix Duarte, R.; Wilks, R. G.; Witte, W.; Bär, M.; Sadewasser, S. Evidence for Chemical and Electronic Non-Uniformities in the Formation of the Interface of RbF-Treated Cu(In,Ga)Se_2 with CdS. *ACS Appl. Mater. Interfaces* **2017**, *9*, 44173–44180.
(25) Solar Frontier Achieves World Record Thin-Film Solar Cell Efficiency of 22.9% http://www.solar-frontier.com/eng/news/2017/1220_press.html (accessed May 25, 2018).
(26) Jia, J. J.; Callcott, T. A.; Yurkas, J.; Ellis, A. W.; Himpsel, F. J.; Samant, M. G.; Stöhr, J.; Ederer, D. L.; Carlisle, J. A.; Hudson, E. A.; Terminello, L. J.; Shuh, D. K.; Perera, R. C. C. First Experimental Results from IBM/TENN/TULANE/LLNL/LBL Undulator Beamline at the Advanced Light Source. *Rev. Sci. Instrum.* **1995**, *66*, 1394–1397.
(27) C. Heske; R. Fink; E. Umbach; W. Riedl; F. Karg. Na-induced Effects on the Electronic Structure and Composition of Cu(In,Ga)Se_2 Thin-film Surfaces. *Appl. Phys. Lett.* **1996**, *68*, 3431–3433.
(28) Yeh, J. J.; Lindau, I. Atomic Subshell Photoionization Cross Sections and Asymmetry Parameters: $1 \leqslant Z \leqslant 103$. *At. Data Nucl. Data Tables* **1985**, *32*, 1–155.

(29) Tanuma, S.; Powell, C. J.; Penn, D. R. Calculations of Electron Inelastic Mean Free Paths. V. Data for 14 Organic Compounds over the 50–2000 eV Range. *Surf. Interface Anal.* **1994**, *21*, 165–176.
(30) Heske, C.; Richter, G.; Chen, Z.; Fink, R.; Umbach, E.; Riedl, W.; Karg, F. Influence of Na and H_2O on the Surface Properties of Cu(In,Ga)Se_2 Thin Films. *J. Appl. Phys.* **1997**, *82* (5), 2411.
(31) Niles, D. W.; Ramanathan, K.; Hasoon, F.; Noufi, R.; Tielsch, B. J.; Fulghum, J. E. Na Impurity Chemistry in Photovoltaic CIGS Thin Films: Investigation with X-Ray Photoelectron Spectroscopy. *J. Vac. Sci. Technol., A* **1997**, *15*, 3044–3049.
(32) Ruckh, M.; Schmid, D.; Kaiser, M.; Schäffler, R.; Walter, T.; Schock, H. W. Influence of Substrates on the Electrical Properties of Cu(In,Ga)Se_2 Thin Films. *Sol. Energy Mater. Sol. Cells* **1996**, *41*, 335–343.
(33) Kylner, A. The Chemical Bath Deposited CdS/Cu(In,Ga)Se_2 Interface as Revealed by X-Ray Photoelectron Spectroscopy. *J. Electrochem. Soc.* **1999**, *146*, 1816–1823.
(34) Granath, K.; Bodegård, M.; Stolt, L. The Effect of NaF on Cu(In, Ga)Se_2 Thin Film Solar Cells. *Sol. Energy Mater. Sol. Cells* **2000**, *60*, 279–293.
(35) Hauschild, D.; Meyer, F.; Pohlner, S.; Lechner, R.; Dietmüller, R.; Palm, J.; Heske, C.; Weinhardt, L.; Reinert, F. Impact of Environmental Conditions on the Chemical Surface Properties of Cu(In,Ga)$(S,Se)_2$ Thin-Film Solar Cell Absorbers. *J. Appl. Phys.* **2014**, *115*, 183707.

(36) Duncan, D. A.; Kephart, J. M.; Horsley, K.; Blum, M.; Mezher, M.; Weinhardt, L.; Häming, M.; Wilks, R. G.; Hofmann, T.; Yang, W.; Bär, M.; Sampath, W. S.; Heske, C. Characterization of Sulfur Bonding in CdS:O Buffer Layers for CdTe-Based Thin-Film Solar Cells. *ACS Appl. Mater. Interfaces* **2015**, *7*, 16382–16386.
(37) Wagner, C. D. Chemical Shifts of Auger Lines, and the Auger Parameter. *Faraday Discuss. Chem. Soc.* **1975**, *60*, 291–300.
(38) Naumkin, A.; Kraut-Vass, A.; Gaarenstroom, S.; Powell, C. NIST X-ray Photoelectron Spectroscopy (XPS) Database, Version 4.1 http://srdata.nist.gov/xps/Default.aspx (accessed Sep 10, 2018).
(39) Moulder, J. F.; Stickle, W. F.; Sobol, P. E.; Bomben, K. D. *Handbook of X-Ray Photoelectron Spectroscopy, Perkin-Elmer Corporation.*; Physical Electronics Division, 1992.
(40) Wojdyr, M. Fityk: A General-Purpose Peak Fitting Program. *J. Appl. Crystallogr.* **2010**, *43*, 1126–1128.
(41) Hauschild, D.; Meyer, F.; Benkert, A.; Kreikemeyer-Lorenzo, D.; Dalibor, T.; Palm, J.; Blum, M.; Yang, W.; Wilks, R. G.; Bär, M.; Reinert, F.; Heske, C.; Weinhardt, L.; Improving Performance by Na Doping of a Buffer Layer—Chemical and Electronic Structure of the In_xS_y:Na/CuIn$(S,Se)_2$ Thin-Film Solar Cell Interface. *Prog. Photovolt. Res. Appl.* **2018**, *26* (5), 359–366.
(42) Schmid, D.; Ruckh, M.; Schock, H. W. Photoemission Studies on Cu(In,Ga)Se_2 Thin Films and Related Binary Selenides. *Appl. Surf. Sci.* **1996**, *103*, 409–429.
(43) Faur, M.; Faur, M.; Jayne, D. T.; Goradia, M.; Goradia, C. XPS Investigation of Anodic Oxides Grown on p-Type InP. *Surf. Interface Anal.* **1990**, *15*, 641–650.
(44) Gullikson, E. M. CXRO X-Ray Interactions With Matter http://henke.lbl.gov/optical_constants/ (accessed Sep 14, 2018).
(45) Weinhardt, L.; Fuchs, O.; Fleszar, A.; Bär, M.; Blum, M.; Weigand, M.; Denlinger, J. D.; Yang, W.; Hanke, W.; Umbach, E.; Heske, C. Resonant Inelastic Soft X-Ray Scattering of CdS: A Two-Dimensional Electronic Structure Map Approach. *Phys. Rev. B* **2009**, *79*, 165305.

(46) A. Meisel; G. Leonhardt; R. Szargan. *Röntgenspektren und chemische Bindung*, 1st edition.; Leipzig Geest & Portig, 1977.
(47) Reichardt, J.; Bär, M.; Grimm, A.; Kötschau, I.; Lauermann, I.; Sokoll, S.; Lux-Steiner, M. C.; Fischer, C.-H.; Heske, C.; Weinhardt, L.; Fuchs, O.; Jung, C.; Gudat, W.; Niesen, T. P.; Karg, F. Inducing and Monitoring Photoelectrochemical Reactions at Surfaces and Buried Interfaces in Cu(In,Ga)(S,Se)$_2$ Thin-Film Solar Cells. *Appl. Phys. Lett.* **2005**, *86*, 172102.
(48) Heske, C.; Groh, U.; Fuchs, O.; Weinhardt, L.; Umbach, E.; Schedel-Niedrig, T.; Fischer, C.-H.; Lux-Steiner, M. C.; Zweigart, S.; Niesen, T. P.; Karg, F.; Denlinger, J. D.; Rude, B.; Andrus, C.; Powell, F. Monitoring Chemical Reactions at a Liquid–Solid Interface: Water on CuIn(S,Se)$_2$ Thin Film Solar Cell Absorbers. *J. Chem. Phys.* **2003**, *119*, 10467.

TOC

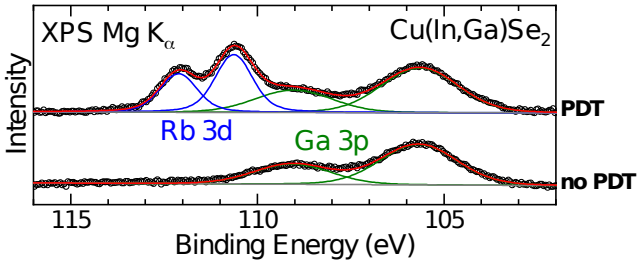
XPS Mg K$_\alpha$
Cu(In,Ga)Se$_2$
Intensity
Rb 3d
Ga 3p
PDT
no PDT
115
110
105
Binding Energy (eV)